

From ATLASGAL to SEDIGISM: Towards a Complete 3D View of the Dense Galactic Interstellar Medium

Frédéric Schuller¹
 James Urquhart^{2,1}
 Leonardo Bronfman³
 Timea Csengeri¹
 Sylvain Bontemps⁴
 Ana Duarte-Cabral⁵
 Andrea Giannetti¹
 Adam Ginsburg⁶
 Thomas Henning⁷
 Katharina Immer⁶
 Silvia Leurini¹
 Michael Mattern¹
 Karl Menten¹
 Sergio Molinari⁸
 Erik Muller⁹
 Alvaro Sánchez-Monge¹⁰
 Eugenio Schisano⁸
 Sümeyye Suri¹⁰
 Leonardo Testi⁶
 Ke Wang⁶
 Friedrich Wyrowski¹
 Annie Zavagno¹¹

¹ Max-Planck-Institut für Radioastronomie, Bonn, Germany

² Centre for Astrophysics and Planetary Science, University of Kent, United Kingdom

³ University of Chile, Departamento de Astronomía, Chile

⁴ Laboratoire d'Astrophysique de Bordeaux, University of Bordeaux, France

⁵ School of Physics, University of Exeter, United Kingdom

⁶ ESO

⁷ Max-Planck-Institut für Astronomie, Heidelberg, Germany

⁸ INAF, Istituto di Astrofisica e Planetologia Spaziali, Rome, Italy

⁹ National Astronomical Observatory of Japan, Tokyo, Japan

¹⁰ University of Cologne, I. Physikalisches Institut, Germany

¹¹ Laboratoire d'Astrophysique de Marseille, France

The ATLASGAL survey has provided the first unbiased view of the inner Galactic Plane at sub-millimetre wavelengths. This is the largest ground-based survey of its kind to date, covering 420 square degrees at a wavelength of 870 μm . The reduced data, consisting of images and a catalogue of $> 10^4$ compact sources, are available from the ESO Science Archive Facility through

the Phase 3 infrastructure. The extremely rich statistics of this survey initiated several follow-up projects, including spectroscopic observations to explore molecular complexity and high angular resolution imaging with the Atacama Large Millimeter/submillimeter Array (ALMA), aimed at resolving individual protostars. The most extensive follow-up project is SEDIGISM, a 3D mapping of the dense interstellar medium over a large fraction of the inner Galaxy. Some notable results of these surveys are highlighted.

The ATLASGAL survey

Many large-scale imaging surveys of the Galactic Plane have recently been conducted. In particular, the Spitzer and Herschel space observatories have delivered an unprecedented view of the Galaxy in the near- to far-infrared range. Nevertheless, the global structure of the Milky Way (number of arms, position of the central bar) is still poorly constrained. Moreover, the life-cycle of interstellar matter is not yet understood in detail. We have made use of the high sensitivity sub-millimetre instruments installed at the Atacama Pathfinder EXperiment (APEX) telescope to conduct several large programmes, aimed at mapping the dense interstellar medium (ISM) on the scale of hundreds of square degrees.

ATLASGAL, the APEX Telescope Large Area Survey of the GALaxy (Schuller et al., 2009), mapped 420 square degrees of the inner Galaxy in sub-millimetre continuum emission. Observations started immediately after the successful commissioning of the Large APEX BOLometer CAMERA (LABOCA; Siringo et al., 2009),

in 2007. Data were collected until 2010. In total, this project used 420 hours of telescope time, shared between ESO, Max-Planck and Chilean time.

The LABOCA data were reduced using the dedicated bolometer analysis (BoA) software; details can be found in Schuller et al. (2009). The most critical step in the processing of ground-based sub-millimetre continuum data is the removal of the sky emission, which is several orders of magnitude brighter than even the brightest astronomical source. Since uniform, extended astronomical emission on spatial scales comparable to the instrument field of view mimics the variations in sky emission, it is also filtered out during the sky removal process. Thus, uniform emission on scales larger than a few arcminutes cannot be properly recovered at this stage. However, the lost information on the distribution of diffuse emission can be recovered by combining the ground-based data with maps observed from space; this is discussed in more detail later.

The astrometric accuracy of the ATLASGAL maps is better than 4 arcseconds, as derived from the dispersion of the offsets measured on reference pointing sources. The uncertainty of the flux density calibration is estimated to be lower than 15%. The root mean square (rms) noise level measured in the emission maps is generally in the range 50–80 mJy/beam, but varies between maps due to weather conditions and the number of times a given area was covered; these variations are illustrated in Figure 1.

The continuum emission measured at 870 μm mostly originates from thermal dust emission, which is almost always

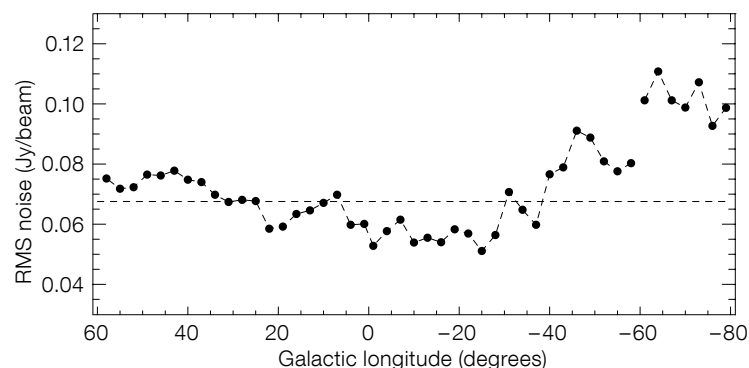
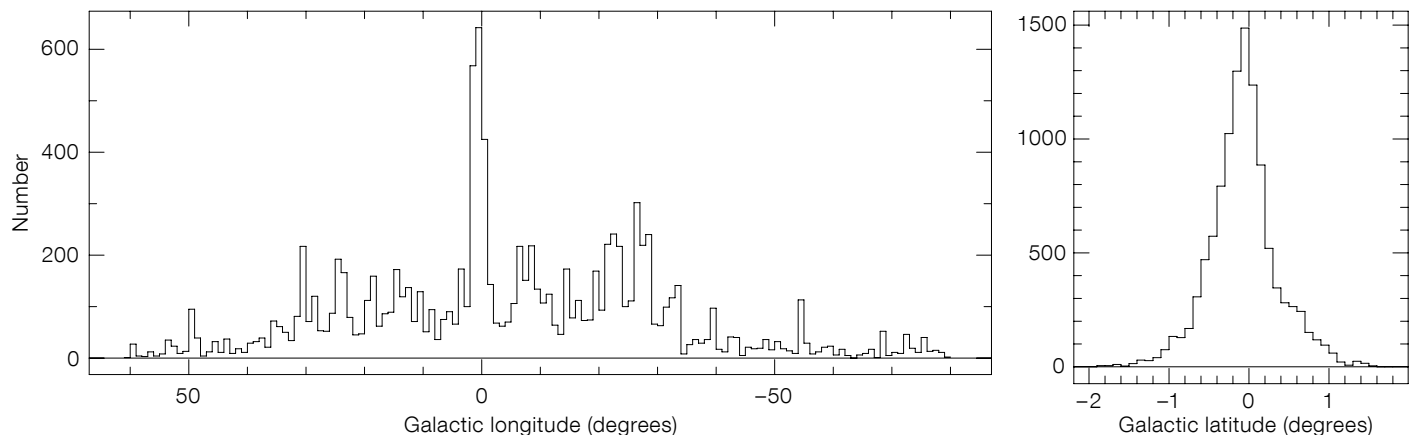


Figure 1. Variation of the RMS noise level with Galactic longitude for the ATLASGAL survey. The average value (68 mJy/beam) is indicated by the horizontal dashed line.



optically thin in the sub-millimetre regime. Therefore, the measured flux density can be directly converted to a total column density along the line of sight. Using typical dust properties and a temperature of 20 K, the ATLASGAL 5- σ sensitivity (250 mJy/beam) corresponds to an H₂ column density of $\sim 1 \times 10^{22}$ cm⁻², equivalent to 10 magnitudes of visual extinction. When distances are known, the integrated flux densities can also be converted to masses: the ATLASGAL survey is sensitive to cold cores with masses below 1 M_{\odot} at 500 pc, and can detect all cores more massive than $\sim 100 M_{\odot}$ at the distance of the Galactic Centre. It is complete across the inner Galaxy to dense clumps more massive than 1000 M_{\odot} .

After completion of a Large Programme like ATLASGAL, the legacy survey data products are ingested into the Phase 3 infrastructure of the ESO Science Archive Facility to make them available to the scientific community¹. We adapted the headers of the ATLASGAL images and the catalogue files to conform to the ESO standards. The files were then uploaded to the ESO archive in January 2016. The weight maps, source masks and catalogue files are all included in the archive. A press release² announced the completion of the ATLASGAL survey and the availability of the data products. The data can also be retrieved from the dedicated server hosted at MPIfR³, where cut-out images and complementary data at other wavelengths are also available.

Compact sources

Two compact source catalogues have been extracted from the data: the Compact Source Catalogue (CSC) was built using

the SExtractor program (see Contreras et al., 2013 and Urquhart et al., 2014a for details); the GaussClump Source Catalogue (GCSC; Csengeri et al., 2014) was generated by running the GAUSSCLUMPS algorithm on modified versions of the images, where emission extended on scales larger than ~ 100 arcseconds has been filtered out using a wavelet decomposition. Therefore, the GCSC is better suited for characterising compact sources, even those embedded within diffuse interstellar material, while the CSC provides a better estimate of the total emission along any given line of sight, and it also contains more extended clumps. The total number of sources is 10 861 in the GCSC, and 10 163 in the CSC.

The distribution of all CSC sources in Galactic coordinates is shown in Figure 2. The distribution in Galactic longitude shows a strong peak towards the Galactic

Figure 2. Distributions of ATLASGAL compact sources in Galactic longitude (left) and Galactic latitude (right).

Centre, while the median of the latitude distribution is at -0.08° , significantly below the Galactic mid-plane. The distributions of integrated fluxes from both catalogues are shown in Figure 3. On average, fluxes from the GCSC are lower than those measured on CSC sources, which can be explained by the filtering of extended emission performed on the images before the extraction of the GCSC sources.

The ATLASGAL CSC catalogue has been cross-matched with a number of surveys that have specifically searched for young massive embedded stars, for example the Red MSX Source (RMS) survey, the 5 GHz VLA CORNISH survey, and the methanol multi-beam (MMB) survey. This has produced a large and representative

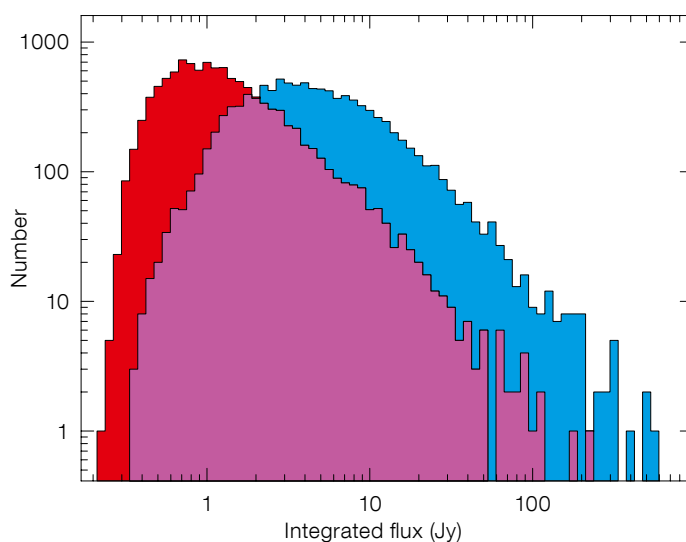


Figure 3. Distribution of integrated fluxes for all ATLASGAL compact sources extracted with GAUSSCLUMPS (in red) and SExtractor (in blue).

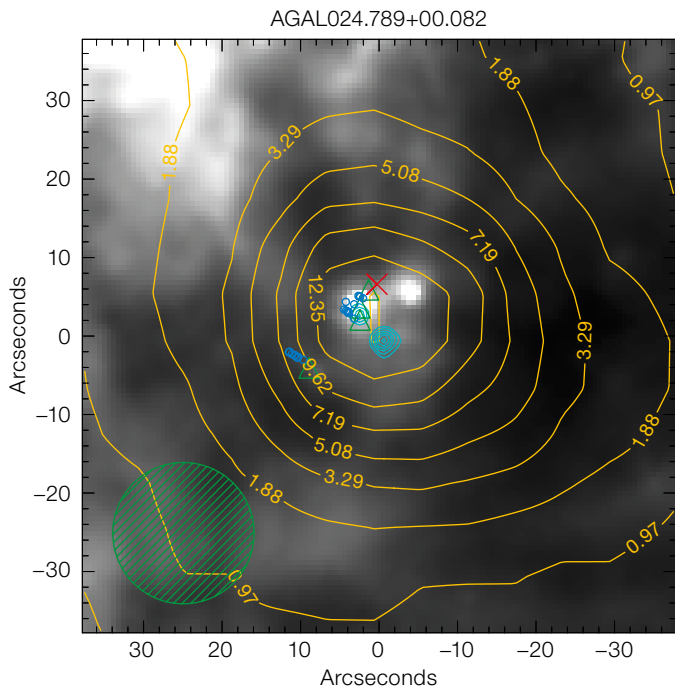


Figure 4. A typical example of a massive star-formation region hosting multiple evolutionary stages. The greyscale image is the $8\ \mu\text{m}$ emission map from Spitzer, while the yellow and cyan contours trace the ATLASGAL $870\ \mu\text{m}$ dust and $5\ \text{GHz}$ radio continuum emission, respectively. The contour labels give the sub-millimetre flux in Jy. The blue circles, green triangles and red cross mark the positions of water masers, methanol masers, and the massive young stellar object, respectively. The LABOCA beam is shown with a dashed circle in the lower-left corner.

500 filamentary structures, with lengths between ~ 2 and $20\ \text{pc}$. High-mass star formation seems to be ongoing within 20% of these filaments, preferentially within the ones with the largest mass-to-length ratios. Moreover, these filaments are predominantly aligned with the Galactic Plane, and associated with the spiral arms. This seems to indicate a direct link between star formation activity and large scale Galactic structure.

On even larger scales, combining ATLASGAL with data from space-based telescopes allows us to recover the extended emission that is filtered out by the processing of ground-based observations. We used the data from the Planck HFI instrument to build maps tracing the distribution of cold dust in the Galactic Plane with an excellent spatial dynamic range, and with an angular resolution ~ 2 times better than the space-based data (Csengeri et al., 2016a). This comparison allowed us to estimate the dense gas fraction in the Galactic Plane; we find an average value of $\sim 2\%$ for the Galaxy. Using simple but realistic assumptions, we could also convert the total flux density measured in the maps to a total mass of molecular gas in the inner Galaxy, finding $\sim 1 \times 10^9 M_{\odot}$, consistent with previous estimates based on CO emission maps (see Heyer & Dame, 2015 for a recent review). Finally, from the total mass and the dense gas fraction, we can estimate an average Galactic star formation rate of $\sim 1.3 M_{\odot} \text{yr}^{-1}$.

Resolving massive clumps with ALMA
In order to better understand the origin of high-mass stars and rich clusters, the earliest phases of star formation need to be characterised in detail. The rich statistics of massive clumps provided by ATLASGAL have allowed us to define a sample of the youngest massive clumps in the inner Galactic Plane. These are the best targets for follow-up observations at sub-arcsecond resolution with ALMA to reveal their protostellar content.

Altogether 46 massive clumps were targeted, where precursors of O-type stars are expected to form. Preliminary results indeed confirm that these massive clumps are associated with the earliest stages of high-mass protostars, and reveal a sample of the most massive dense cores

sample of massive star-forming (MSF) clumps, ideal to study the properties of the embedded objects and their natal environments (Urquhart et al., 2014b). In total, we have identified ~ 1300 MSF clumps that cover the important stages of the formation of massive stars: from the formation of the protostar traced by the association with methanol masers; through the mid-infrared bright massive young stellar object (MYSO) stage; to the arrival on the main sequence and the formation of an H II region. Approximately a third of these MSF clumps are associated with two or more different evolutionary stages, illustrating the complexity of some of these regions (see Figure 4 for an example).

A comparison with less active clumps reveals that high mass star formation is strongly correlated with the regions of highest column density in spherical, centrally condensed clumps with masses $\geq 1000 M_{\odot}$. We find no significant differences, however, between the samples of methanol masers, MYSOs and H II regions in the structure of the clumps or the relative locations of the embedded stars with respect to the peak column density within the clumps. This suggests that massive stars tend to form towards the centre of their host clumps and that the structure of the clump is set before

the onset of star formation and changes little as the embedded object evolves towards the main sequence (see Urquhart et al., 2014b for more details).

Analysis of the physical properties of the clumps does reveal systematic increases in the temperatures, luminosities and the amount of turbulence present in the gas as a function of evolution of the embedded objects, indicating that feedback from the embedded stars is having an impact on their local environment. We also find a strong linear correlation between the clump mass and the bolometric luminosity, with the most massive stars forming in the most massive clumps. Comparing the luminosities of the embedded compact H II regions and MYSOs to the expected cluster luminosity, we find they are underluminous, indicating that the lower mass companions have yet to form and suggesting a scenario where the high mass stars in a cluster form first.

Extended emission

As a blind survey, ATLASGAL provides a unique dataset from which to compile an unbiased catalogue of filamentary structures throughout the Galaxy. Li et al. (2016) used the survey images to identify filament candidates in the Galactic Plane through their continuum emission at $870\ \mu\text{m}$. They identified more than

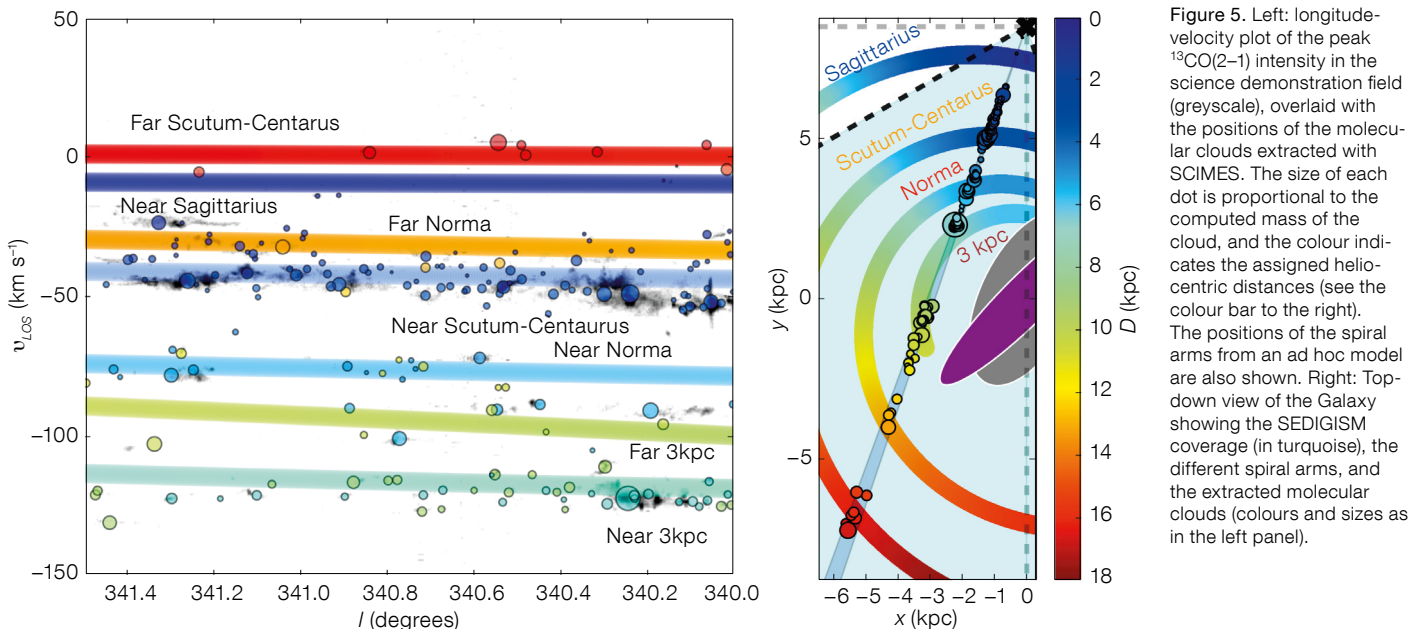


Figure 5. Left: longitude-velocity plot of the peak $^{13}\text{CO}(2-1)$ intensity in the science demonstration field (greyscale), overlaid with the positions of the molecular clouds extracted with SCIMES. The size of each dot is proportional to the computed mass of the cloud, and the colour indicates the assigned heliocentric distances (see the colour bar to the right). The positions of the spiral arms from an ad hoc model are also shown. Right: Top-down view of the Galaxy showing the SEDIGISM coverage (in turquoise), the different spiral arms, and the extracted molecular clouds (colours and sizes as in the left panel).

and protostars known to date (Csengeri et al., in prep.).

Spectroscopic follow-ups

Continuum observations can be affected by line-of-sight projection effects, which make it difficult to determine whether a detected structure is a single, coherent object. Spectroscopic follow-up observations are crucial to measure (local standard of rest) radial velocities (v_{lsr}) of objects detected in the continuum, and to determine their kinematic distances, essential for computing the masses and physical sizes of the clumps. Therefore, an extensive programme of follow-up observations in ammonia lines was started; such observations have the advantage of providing gas temperatures in the clumps, by combining the information about the simultaneously observed (1,1) and (2,2) ammonia inversion transitions. More than 1000 sources have been observed with the Effelsberg and Parkes telescopes (Wienen et al., 2012, 2015). Distances were determined based on the measured velocities and the analysis of archival HI data to resolve the distance ambiguities. The measured temperatures and line-widths track the evolution of the clumps. In addition, using the Herschel Space Observatory, water absorption lines from diffuse line-of-sight clouds towards ATLASGAL clumps were used to determine distances to infrared-dark clouds (Giannetti et al., 2015), leading to the

surprising result that a fraction of those are situated in the far distance, and are therefore more massive than originally estimated.

Further spectroscopic follow-ups consist of millimetre line surveys of a few hundred clumps with the IRAM 30-metre, Mopra and APEX telescopes. Giannetti et al. (2014) analysed the CO isotopologue lines from these surveys to determine CO column densities and to study, in conjunction with the ATLASGAL dust column densities, the gas depletion in the clumps. This study revealed that CO depletion in high-mass clumps seems to behave as in the low-mass regime, with less evolved clumps showing larger values for the depletion than their more evolved counterparts, and increasing for denser sources. Finally, SiO, which is usually associated with shocks and traces ongoing star formation deeply embedded in the clumps, was found in a large fraction of the clumps (Csengeri et al., 2016b).

The SEDIGISM survey

Molecular line data not only provide a way to determine distances, but also deliver strong constraints on the gas excitation, chemical abundances, and the properties of interstellar turbulence. In order to complement existing molecular line surveys, such as the Galactic Ring

Survey (Jackson et al., 2006) in the northern hemisphere, and older surveys at low angular resolution, we have undertaken the SEDIGISM survey (Structure, Excitation, and Dynamics of the Inner Galactic InterStellar Medium). It covers 78 square degrees of the southern Galactic Plane: $-60 \leq l \leq +18$ degrees, with $|b| \leq 0.5$ degrees, at 30 arcsecond resolution. The data cover the frequency range from 217 to 221 GHz, at 0.1 km s^{-1} resolution, which includes the $^{13}\text{CO}(2-1)$ and $\text{C}^{18}\text{O}(2-1)$ lines. These lines are usually optically thin in the Galactic ISM, making them ideal tools to trace the cold, dense interstellar medium. The observations started in 2013, and were completed by the end of 2015. A dedicated reduction pipeline has been developed and the systematic processing of this prodigious amount of data (over 10^7 independent spectra) is ongoing.

Molecular clouds and giant complexes

Molecular line emission is crucial to reveal the 3D distribution of the gas in the Galaxy, and essential to link the compact dense gas clumps seen in the dust continuum emission of ATLASGAL to the large scales of giant molecular clouds and complexes that host them. In order to identify giant molecular clouds (GMCs), we have used the SCIMES algorithm (Colombo et al., 2015) on the $^{13}\text{CO}(2-1)$ data cube towards a science demonstration field, covering 1.5 square degrees.

We extracted a total of 182 molecular clouds, of which 58 are large complexes showing sub-structure. We have derived their kinematic distances using the Galactic rotation model of Brand & Blitz (1993), along with standard methods for resolving the ambiguity between near and far distances (e.g. the existence of HI self-absorption, infrared [IR] dark clouds, and parallax measurements in the literature). The distance distribution of these 182 molecular clouds traces the spiral structure of the Galaxy, providing an accurate view of the position of the near Scutum-Centaurus arm, the near and far Norma arm, and the near and far 3 kpc arm (Figure 5).

Having determined the distances to all the clouds, we estimated their physical properties: size, mass, surface density and virial parameter. We find that most clouds in our sample are stable, with a median virial parameter of ~ 2 . We observe a trend of decreasing virial parameters with increasing cloud masses. A similar trend is observed for the dense clumps (as traced by ATLASGAL) embedded in the clouds. This indicates that the most massive clouds and clumps are the most gravitationally unstable, i.e. the most likely to collapse and form stars. Within the science demonstration field, we also find that 18 dense clumps (within 12 molecular clouds) are associated with high-mass star formation (HMSF) tracers; these tend to be among the most massive and unstable dense clumps and clouds of our sample (see Figure 6), and they are preferentially located within the spiral arms.

Although these are still preliminary results, based on $\sim 2\%$ of the survey data, they demonstrate the potential of the full SEDIGISM survey as a high angular resolution spectral line survey to provide a detailed yet global view of the distribution of molecular clouds and star formation in the inner Milky Way.

Filamentary structures

The SEDIGISM data are perfectly suited for confirming the nature of filament candidates, and for separating structures overlapping along the line of sight, because the $^{13}\text{CO}(2-1)$ and $\text{C}^{18}\text{O}(2-1)$ lines are excited in relatively low density gas, but are less affected by high opacities than lines from the main ^{12}CO isotopologue.

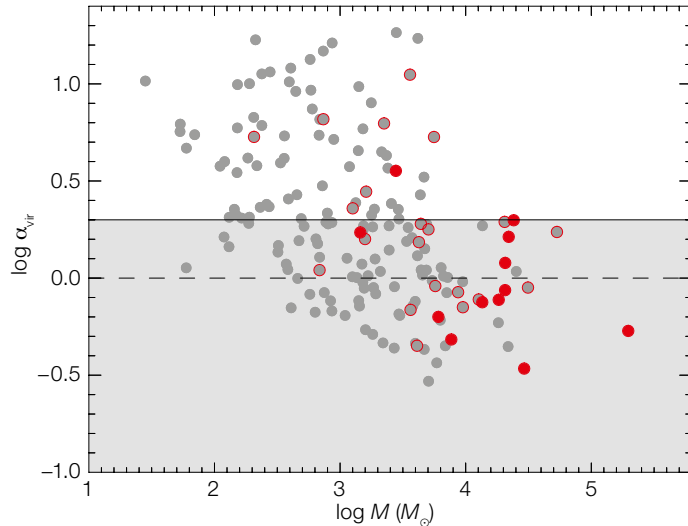


Figure 6. Virial parameter (α_{vir}) as a function of GMC mass. GMCs associated with high mass star formation (HMSF) tracers are indicated with red filled circles. GMCs with an ATLASGAL match but no HMSF tracer are shown as grey circles with a red outline. Grey shading indicates the region where clouds are unstable and likely to be collapsing.

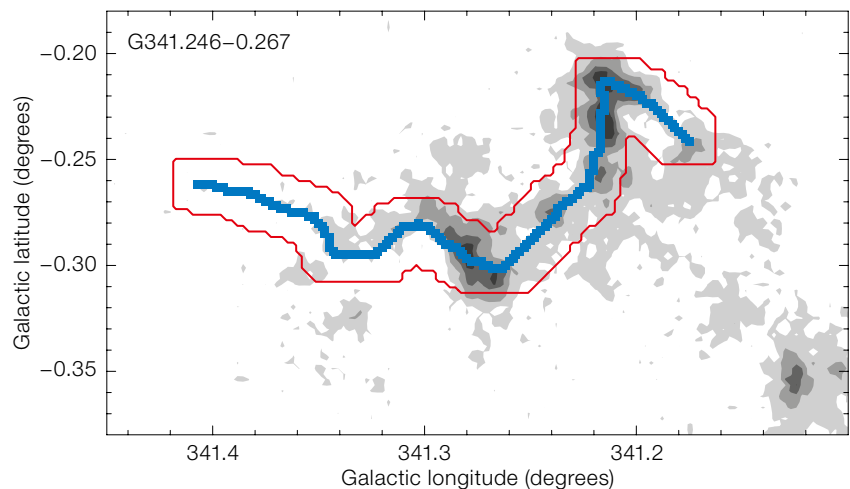
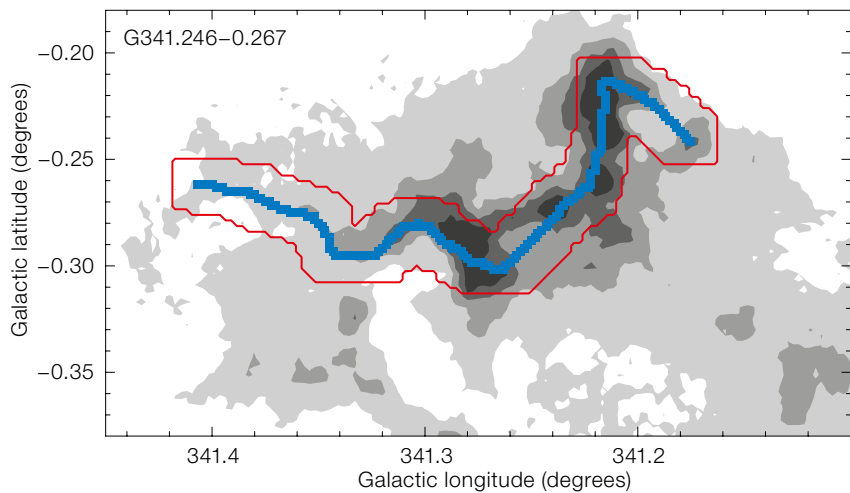


Figure 7. Emission maps of $^{13}\text{CO}(2-1)$ (upper) and $\text{C}^{18}\text{O}(2-1)$ (lower) towards G341.246-0.267, integrated over the velocity range -48 to -41 km s^{-1} . The solid blue line marks the main spine of the

filament identified on the ATLASGAL data. The thin red line marks the dilation box used to compute the length and the mass of the filament.

Moreover, molecular line data allow us to derive the distances and physical properties of the filaments: mass, size, velocity dispersion and line-to-mass ratio.

In Figure 7, we show the $^{13}\text{CO}(2-1)$ and $\text{C}^{18}\text{O}(2-1)$ data for G341.246–00.267, one of the filament candidates extracted from ATLASGAL by Li et al. (2016). Using the SEDIGISM data, we first verified the coherence in velocity of the filament candidate. We analysed the velocity structure and compared the morphology of the molecular line emission with that of the dust to verify their association. For G341.246–00.267, we found a coherent structure at a central velocity of -44.6 km s^{-1} , with an emission line full width at half maximum (FWHM) of 3.6 km s^{-1} .

To estimate the mass of the filament, we integrated the ^{13}CO column density over the extent of the filament, both spatially and in velocity (see Figure 7). In order to compute column densities, we used a $^{13}\text{CO}(2-1)$ -to- H_2 X-factor that we derived from comparing the SEDIGISM data with a column density map built from Hi-GAL (Molinari et al. 2010). We found that $X^{13}\text{CO}(2-1) \approx 1 \times 10^{21} \text{ cm}^{-2} (\text{K km s}^{-1})^{-1}$ (see Schuller et al., 2016 for details). We then computed the mass of the filament by converting the H_2 column densities to total gas mass, using standard factors for the Galactic ISM. This results in a mass of $22.4 \times 10^3 M_{\odot}$ for G341.246–00.267, located at a distance of 3.6 kpc.

The gravitational stability of a filament can be inferred by comparing its mass per unit length, (M/l) with the virial mass per unit length given by twice the ratio of the 1-dimensional velocity dispersion squared of the average molecular gas and the gravitational constant, G . For the 21.3-pc-long filament G341.246–00.267, we measured a mass per unit length of $1050 M_{\odot} \text{ pc}^{-1}$, or about twice the virial mass per unit length, which is $510 M_{\odot} \text{ pc}^{-1}$. Therefore, the filament is critical and is likely to undergo radial collapse. However, our measurements of masses include several uncertainties: the $X^{13}\text{CO}(2-1)$ factor has an uncertainty of at least a factor of two; additionally, opacity effects were not taken into account, which can lead to an underestimate of the true column density in the densest parts of the filament.

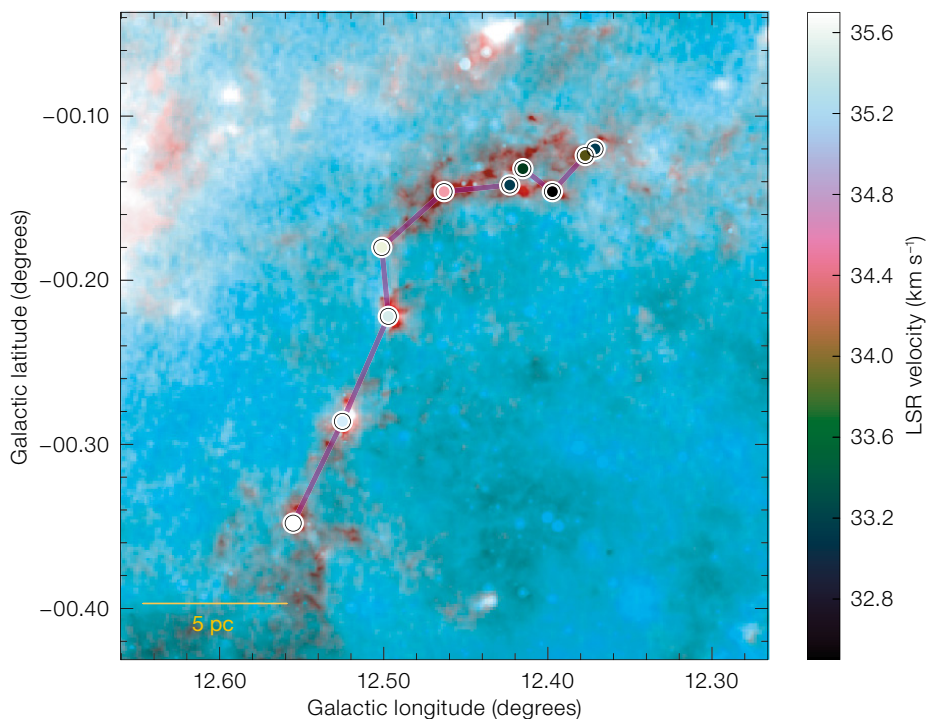


Figure 8. A two-colour view of an example filament identified by Wang et al. (2016). Cyan shows the Spitzer 24 μm emission on a logarithmic scale, and red shows the ATLASGAL + Planck 870 μm emission on a linear scale. The circles depict dense BGPS sources with fill colour coded velocity as shown by the colour bar. The filament is outlined by the connected BGPS sources (purple line).

The SEDIGISM data are likely to include many more filaments than those identified in the continuum images. The velocity information contained in spectroscopic datasets automatically solves the problem of blending of unrelated structures along the line of sight, which severely affects continuum surveys. We have used the DisPerSE algorithm (Sousbie, 2011) to directly search for filamentary structures in the $^{13}\text{CO}(2-1)$ data-cube for the science demonstration field. We identified 145 different velocity-coherent structures; 33 of them have an aspect ratio larger than five, making them the best filament candidates. While some of these filaments are also identified in the ATLASGAL continuum images, DisPerSE is sensitive to different structures, and in some cases it reveals that the filaments identified in the continuum are composed of several sub-structures. The typical lengths and widths of the filaments identified in the ^{13}CO data are 4.7–14.1 pc and 1.3–3.8 pc, respectively.

Recent studies have revealed some very long filaments in the Milky Way (e.g., Wang et al., 2015), with lengths up to ~ 100 pc. They are on the upper end of the filamentary hierarchy of the Galactic ISM. Their association with respect to the Galactic structure and their role in star formation are of great interest from both observational and theoretical points of view.

With SEDIGISM adding velocity information to the $> 10^4$ targets in the ATLASGAL compact source catalogue, the combined 3D position-position-velocity (PPV) catalogue will provide a valuable tool for extracting large-scale velocity-coherent filaments. Wang et al. (2016) have developed a new method to automate the filament-finding process from such 3D discrete data point collections. The method is based on a customised minimum spanning tree algorithm, which connects physically related voxels in PPV space (Figure 8). Applying this method to the Bolocam Galactic Plane Survey (BGPS) spectroscopic catalogue, Wang et al. (2016) have made the first census of the longest filaments in the northern Galactic Plane, where they identified 54 large-scale filaments, with masses in the range $\sim 10^3$ to $10^5 M_{\odot}$, and lengths up to ~ 300 pc. The filaments concentrate along major spiral arms and are widely

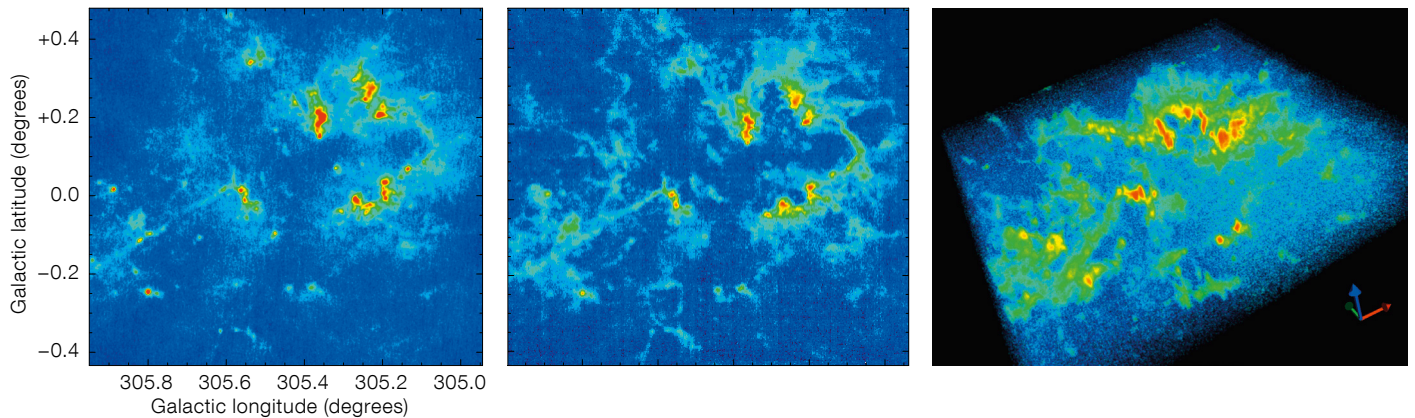


Figure 9. The G305 star-forming complex, as seen with ATLASGAL combined with Planck data (left). The middle panel shows the integrated $^{13}\text{CO}(2-1)$ emission observed with SEDIGISM, and the right panel shows a 3D rendering of the datacube, produced with the GLnemo2⁴ interactive visualisation software.

distributed across the Galactic Disc, with 50% located within ± 20 pc of the Galactic mid-plane. 27 % of the filaments seem to run in the centre of spiral arms, and may form the “bones” of the Galactic structure. On the order of 1 % of the molecular ISM appears to be confined in large filaments. Statistically, the formation of massive stars seems to happen preferentially in large filaments.

Applying the same method to the ATLASGAL+SEDIGISM 3D source catalogue will allow us to complete the census of large filaments in the inner Galaxy, and to deliver a comprehensive filament catalogue, useful for a quantitative comparison with models of the Galactic spiral structure and numerical simulations.

Triggered star formation

Star formation is often observed at the edges of ionised (H II) regions. Recent statistical studies (for example Kendrew et al., 2016) have shown that these regions have a clear impact on their surroundings by promoting star formation. However, many questions remain about how this constructive feedback occurs. Studying the relation between the molecular material that surrounds H II regions and the young sources observed at their edges may help to answer some of the questions.

Molecular material is observed at the edges of H II regions distributed in a shell. The 2D or 3D distribution of this material is still debated (e.g. Beaumont

& Williams, 2010). The 3D visualisation of molecular surveys offers a unique opportunity to make progress in this field, since it becomes possible to visualise the distribution of the different components (molecular, ionised, young sources and cores) along the line of sight and to investigate their relationship.

Figure 9 shows the distribution of the $^{13}\text{CO}(2-1)$ emission over the Galactic H II region G305. Seen face-on (middle panel), the CO emission surrounds the ionised gas. The molecular emission is highly structured with a large number of dense cores. These cores represent the potential sites of high-mass star formation. In 3D (right panel), the spatial distribution is revealed, spanning a range of more than 20 km s^{-1} in velocity. This example shows that the distribution of the densest material and clumps is strongly non-isotropic, suggesting that the interaction between the ionised gas and the surrounding medium can be more efficient under specific conditions. Studying star formation around H II regions with 3D visualisation offers new perspectives in the study of contaminants along the line of sight, since molecular clumps not associated with ionised regions can easily be separated. The SEDIGISM survey, covering a total area of 78 square degrees, thus provides highly valuable data to conduct this kind of study on a large number of Galactic star-forming complexes.

The SEDIGISM survey will deliver an important legacy dataset for understanding the kinematic structure of the dense gas in our Galaxy. Our early work has shown the wide variety of science advancements possible, even with data covering only a tiny fragment of the

Galactic Plane. The full survey will greatly improve our current view of Galactic structure and star formation.

Acknowledgements

APEX is a collaboration between the Max-Planck-Institut für Radioastronomie, ESO and the Onsala Space Observatory.

References

- Beaumont, C. N. & Williams, J. P. 2010, *ApJ*, 709, 791
- Brand, J. & Blitz, L. 1993, *A&A*, 275, 67
- Colombo, D. et al. 2015, *MNRAS*, 454, 2067
- Contreras, Y. et al. 2013, *A&A*, 549, A45
- Csengeri, T. et al. 2014, *A&A*, 565, A75
- Csengeri, T. et al. 2016a, *A&A*, 585, A104
- Csengeri, T. et al. 2016b, *A&A*, 586, A149
- Giannetti, A. et al. 2014, *A&A*, 570, A65
- Giannetti, A. et al. 2015, *A&A*, 580, L7
- Heyer, M. & Dame, T. M. 2015, *ARA&A*, 53, 583
- Jackson, J. M. et al. 2006, *ApJS*, 163, 145
- Kendrew, S. et al. 2016, *ApJ*, 825, 142
- Li, G.-X. et al. 2016, *A&A*, 591, A5
- Molinari, S. et al. 2010, *A&A*, 518, L100
- Schuller, F. et al. 2009, *A&A*, 504, 415
- Schuller, F. et al. 2016, submitted to *A&A*
- Siringo, G. et al. 2009, *A&A*, 497, 945
- Sousbie, T. 2011, *MNRAS*, 414, 350
- Urquhart, J. et al. 2014a, *A&A*, 568, A41
- Urquhart, J. et al. 2014b, *MNRAS*, 443, 1555
- Wang, K. et al. 2015, *MNRAS*, 450, 4043
- Wang, K. et al. 2016, *ApJS*, in press, arXiv:1607.06452
- Wienen, M. et al. 2012, *A&A*, 544, A146
- Wienen, M. et al. 2015, *A&A*, 579, A91

Links

- ¹ Access to ATLASGAL Phase 3 data release: http://archive.eso.org/wdb/wdb/adp/phase3_main/form?phase3_collection=ATLASGAL&release_tag=1
- ² ESO Press Release: <http://www.eso.org/public/news/eso1606/>
- ³ ATLASGAL webpage: <http://atlasgal.mpifr-bonn.mpg.de>
- ⁴ GLnemo2 interactive visualization 3D program for N-body snapshots: <http://projets.lam.fr/projects/glnemo2>